Microelectronic Engineering 110 (2013) 329–334

Contents lists available at SciVerse ScienceDirect

Microelectronic Engineering

journal homepage: www.elsevier.com/locate/mee

Effect of synthesis conditions on the properties of citric-acid coated iron oxide nanoparticles

L. Li [a], K.Y. Mak [a], C.W. Leung [b], K.Y. Chan [c], W.K. Chan [c], W. Zhong [d], P.W.T. Pong [a,*]

[a] Department of Electrical and Electronic Engineering, The University of Hong Kong, Hong Kong
[b] Department of Applied Physics, Hong Kong Polytechnic University, Hong Kong
[c] Department of Chemistry, The University of Hong Kong, Hong Kong
[d] Department of Physics, Nanjing University, China

ARTICLE INFO

Article history:
Available online 26 February 2013

Keywords:
Magnetic nanoparticle
Citric acid
Size
Temperature

ABSTRACT

Citric acid is a widely accepted coating material in nanoparticle fabrication for biomedical applications while iron oxide is one popular magnetic material with excellent properties for use in nanoparticle form. However, the effect of synthesis conditions on the properties of iron oxide nanoparticles is not sufficiently understood. Here, citric-acid coated iron oxide nanoparticles were synthesized based on the co-precipitation method through both one-step and two-step process, respectively. The citric acid was added at different stages, and various coating temperatures were used in the two-step process. The nanoparticles were characterized by multiple techniques including Fourier transform infrared spectroscopy, transmission electron microscopy, dynamic light scattering, thermogravimetric analysis, and vibrating sample magnetometry. It was found that the addition of citric acid at different stages can alter the nanoparticle core size, while the coating temperature affects citric acid adsorption around nanoparticles surface and alters the nanoparticle hydrodynamic size. The effect of citric-acid coating on the magnetic behavior was also investigated on 9 nm and 25 nm iron oxide nanoparticles.

1. Introduction

Magnetic nanoparticles have attracted broad attention due to their potential biomedical applications, such as contrast agents for magnetic resonance imaging (MRI), [1] heating mediators for cancer therapy (hyperthermia), [2] and magnetic labels for biosensing [3]. The specific nanoparticle properties must be tailored to each application to obtain the desired results. Magnetic nanoparticles are generally required to be superparamagnetic, with sufficient magnetic saturation, and a small size comparable to the analytes of interest [4].

Iron oxide is one popular magnetic material with excellent properties for use in nanoparticle form [5,6]. In recent decades, multiple iron oxide nanoparticle synthesis methods have been reported in literature including co-precipitation, thermal decomposition, micro-emulsion, hydrothermal synthesis, sono-chemical synthesis, and so on [7–9]. Of these techniques, co-precipitation is a facile and convenient way to fabricate iron oxide nanoparticles with size less than 20 nm. To ensure biocompatibility and prevent agglomeration, iron oxide nanoparticles are usually coated with biocompatible organic or inorganic materials. However, one of the main challenges for the use of the magnetic nanoparticles is to find a good method to functionalize the surface of nanoparticles with the appropriate chemicals [10]. To impart additional functionality and/or conjugate with biologically active agents, iron oxide nanoparticles usually bear functional groups on their surfaces, such as phosphates, sulphates, and carboxylates. Of these functional groups, carboxylate is the strongest binder [11]. On the other hand, some binding affinity may be lost through steric hindrances by large surfactant molecules or long polymer chains, which could be easily overcome with the use of small molecules [12]. Among various small molecules, citric acid ($C_6H_8O_7$), a biocompatible short-chained tri-carboxylic acid, has been extensively used for the preparation of aqueous stable iron oxide nanoparticles for biomedical applications [12–19]. Accordingly, citric acid can be adsorbed onto the surface of the iron oxide nanoparticles by coordinating via one or two of the carboxylate functionalities, leaving at least one carboxylic acid group exposed, making the nanoparticle surface hydrophilic, preventing particle agglomeration, and providing functional groups to be used for further surface derivation [20]. Citric acid has been employed commercially as the coating surfactant of iron oxide nanoparticles, such as in the MRI contrast agent VSOP C184 [13]. Citric-acid coated iron oxide nanoparticles have also been widely studied for their applications in drug delivery, targeted cellular imaging, hyperthermia, and biodetection [12,14–19]. During synthesis, nanoparticle coating can be applied through either a one-step process, where the surfactant

* Corresponding author. Tel.: +852 2857 8491(0); fax: +852 2559 8738.
E-mail address: ppong@eee.hku.hk (P.W.T. Pong).

0167-9317/$ - see front matter © 2013 Elsevier B.V. All rights reserved.
http://dx.doi.org/10.1016/j.mee.2013.02.045

is added during the particle nucleation and growth [21,22], or via a two-step process where the surfactant coating is applied independently after nanoparticle synthesis [23]. Since the citrate ions are known to interfere with the formation and growth of iron oxide nanoparticles, [21] and process temperature has been found to impact the nanocrystal surface ligand dynamics, [24] it is worthwhile to investigate the influences of the synthesis conditions on the nanoparticles. This is a critical and fundamental work to characterize the synthesis of magnetic nanoparticles in order to optimize their resulting properties.

Here, we have synthesized citric-acid coated iron oxide nanoparticles using the co-precipitation method through both a one-step and two-step coating process. The effects introduced by different synthesis conditions, adding the citric acid at different stages and using various coating temperatures in two-step process, are then compared. The impact of the citric-acid coating on the magnetic behavior is also investigated on uncoated iron oxide cores with different sizes.

2. Experiments

2.1. Materials

Ferric chloride hexahydrate ($FeCl_3 \cdot 6H_2O$, $\geqslant$99%), ferrous sulfate heptahydrate ($FeSO_4 \cdot 7H_2O$, $\geqslant$99.0%), sodium hydroxide ($\geqslant$98%), and citric acid ($\geqslant$98%) were purchased from Sigma–Aldrich (USA). All chemicals were used as received. The uncoated iron oxide nanoparticles with size close to 9 nm (U9) were supplied by Liquids Research, Ltd (UK). The uncoated iron oxide nanoparticles with size close to 25 nm (U25) were purchased from Nanostructured and Amorphous Materials, Inc. (USA).

2.2. Nanoparticle synthesis

Our syntheses were based on the co-precipitation method. Fifty milliliter each of $FeSO_4 \cdot 7H_2O$ and $FeCl_3 \cdot 6H_2O$ were mixed together in a molar ratio of 1:2, which was added drop-wise into 200 ml sodium hydroxide (1.8 M) aqueous solution at 80 °C with vigorous mechanical stirring. The reaction continued for 15 min, and then the black precipitates were obtained as uncoated iron oxide nanoparticles (U0). The coating of citric acid was then conducted through three different ways of adding citric acid. 1st method (pre-addition method): the citric acid was pre-added into the ferrous and ferric solution, and then the mixture was added drop-wise into the aqueous solution of sodium hydroxide. The reaction proceeded at 80 °C for 15 min, then at 90 °C for 1 h under vigorous stirring. The final products were retrieved by magnetic decantation, and then washed with DI water. 2nd method (post-addition method): the citric acid was added when the precipitation of uncoated iron oxide nanoparticles occurred. The reaction then proceeded at 90 °C for 1 h under rigorous stirring. The final products were retrieved by magnetic decantation, and washed with DI water. 3rd method (two-step method): a two-step process, initial synthesis of uncoated nanoparticles and a post-synthesis coating of citric acid. First, the uncoated iron oxide nanoparticles synthesized as previously described were collected by magnetic decantation, washed with DI water, and lyophilized. Second, these uncoated nanoparticles powders were re-dispersed in 200 ml DI water under sonication, and then the slurry was heated to a set temperature followed by the addition of citric acid. The coating reaction proceeded for 1 h at the set temperature under vigorous stirring. The final products were retrieved by magnetic decantation and washed with DI water. The citric acid coating concentration (0.5 g/ml) was held constant for each method. The samples are designated by their fabrication method, coating temperature, and core size, as summarized in Table 1. Samples C1 and C2 were obtained by using the 1st method and 2nd method, respectively. Samples C3-U0-90, C3-U0-70, C3-U0-50, and C3-U0-30 were obtained by using the 3rd method under different coating temperatures. Samples C3-U9-90 and C3-U25-90 were obtained by coating the commercially purchased uncoated nanoparticles with citric acid using the post-synthesis coating process (3rd method) at 90 °C with sizes of 9 nm (U9) and 25 nm (U25), respectively.

2.3. Nanoparticle characterization

The presence of characteristic functional groups coated on the nanoparticle surfaces was determined using Fourier transform infrared spectroscopy (FT-IR). The FT-IR spectra of the samples were obtained with a Shimadzu FTIR-8300 spectrometer using KBr pellets. The size and morphology of the samples were observed by transmission electron microscopy (TEM, Philips CM100). The hydrodynamic size of the nanoparticles in water were measured by dynamic light scattering (DLS) using a Malvern Zetasizer 3000 (Malvern, UK). The magnetic property of the lyophilized sample powders was measured at room temperature by using a vibrating sample magnetometer (VSM, Lakeshore VSM 7400). The magnetization was measured over a range of applied field from −10,000 Oe to 10,000 Oe. The iron oxide composition was determined by using thermal gravimetric analysis (TGA, Perkin-Elmer TGA-7). The mass loss of 5–10 mg of lyophilized sample was monitored under N_2 at temperatures from 50 °C to 600 °C at a rate of 50 °C/min.

3. Results and discussion

Successful citric-acid encapsulation of the iron oxide nanoparticles, synthesized using the methods as described in the experimental section, was confirmed by the FT-IR results. Fig 1 shows the representative FT-IR spectrums of the citric acid coated particles (C1, C2, C3-U0-90, C3-U9-90, and C3-U25-90). The peaks at around 570 cm^{-1} indicate the presence of an iron oxide skeleton in all the samples. The peaks near 1630 cm^{-1} and 1415 cm^{-1}, representing carboxylate (COO^-) stretching, were found in all the citric acid coated samples in our experiments. The presence of these peaks is evidence of the formation of the citric acid coating around the iron oxide cores [12,25,26].

3.1. Influence of adding citric acid at different stages

Representative TEM images of the citric-acid coated iron oxide nanoparticles synthesized under similar temperatures using each of three encapsulation techniques (C1, C2, and C3-U0-90), as well as the uncoated nanoparticles (U0), are shown in Fig. 2. Through one-step fabrication techniques (1st method and 2nd method), sample C1 (Fig. 2a) and C2 (Fig. 2b) show an average size of 6 nm and 11 nm, respectively. The two-step synthesized (3rd method) sample C3-U0-90 (Fig. 2c), and the uncoated sample U0 (Fig. 2d) displayed similar spherical morphology with a size around 13 nm, indicating that the post-synthesis coating of citric acid as the surfactant after the synthesis of iron oxide nanoparticles has no significant effect on the particle size. This observation is consistent with the experimental results reported previously [25]. For the iron oxide nanoparticles synthesized using the co-precipitation method, it is known that there are two stages included in this process, nucleation and growth [27]. Compared to the two-step sample C3-U0-90, the smaller particle size of C2 should be attributed to the immediate presence of citric acid after the precipitation of nanoparticles, since the adsorption of citrate ions on the nanoparticle surfaces hinders particle growth after nucleation [25]. The

Table 1
Fabrication conditions of citric coated and uncoated iron oxide nanoparticles.[a]

Nomenclature	Reaction type	Synthesis temp	Coating temp
U0	Uncoated	80	N/A
C1	1st method (pre-addition method)	80, 90	–
C2	2nd method (post-addition method)	80	90
C3-U0-90	3rd method (2-step method)	80	90
C3-U0-70	3rd method (2-step method)	80	70
C3-U0-50	3rd method (2-step method)	80	50
C3-U0-30	3rd method (2-step method)	80	30
C3-U25-90	3rd method (post coating)	N/A	90
C3-U9-90	3rd method (post coating)	N/A	90

[a] Samples C1 and C2 were obtained by using the 1st method and 2nd method, respectively. Samples C3-U0-90, C3-U0-70, C3-U0-50, and C3-U0-30 were obtained by using the 3rd method under different coating temperatures (90 °C, 70 °C, 50 °C, and 30 °C). Samples C3-U9-90 and C3-U25-90 were obtained by coating the uncoated nanoparticles of different sizes (average diameters of 9 nm and 25 nm) with citric acid using the post coating process of 3rd method under the coating temperature of 90 °C.

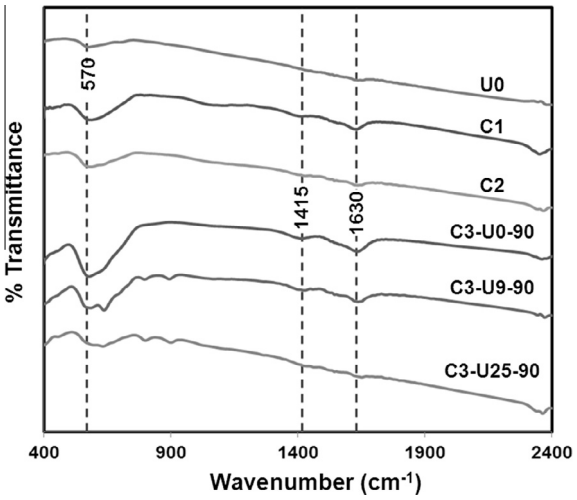

Fig. 1. FT-IR spectra of citric acid coated (C1, C2, C3-U0-90, C3-U9-90, and C3-U25-90) and uncoated (U0) iron oxide nanoparticles.

ultra-small size of C1 should be due to the presence of citric acid during the nucleation step, since the citric acid was pre-added into the ferrous and ferric solutions before the co-precipitation reaction started. The adsorption of citrate ions on the nuclei surfaces can effectively inhibit the growth of the nuclei, [21] which causes the final product C1 with much smaller sizes (6 nm) than samples C2 and C3-U0-90. Additionally, the iron oxide nanoparticles in sample C2 displayed a less spherical morphology than the other three samples. Since the shape of the iron oxide nanoparticles can be affected by the pH value during sample preparation, [16] the less spherical morphology of sample C2 might be due to the pH change caused by the addition of citric acid during particle growth. The mechanism of this phenomenon needs further study.

3.2. Influence of coating temperature in two-step process

The effect of different coating temperature in the two-step process (3rd method) on the adsorption of citric acid around particle surface and the particle hydrodynamic size were studied using TGA and DLS, respectively. The citric-acid coated samples C3-U0-90, C3-U0-70, C3-U0-50, and C3-U0-30 were synthesized using the 3rd method using different post-synthesis coating temperatures of 90 °C, 70 °C, 50 °C and 30 °C, respectively. The weight percentage of the iron oxide cores in the samples C3-U0-90, C3-U0-70, C3-U0-50, and C3-U0-30 were approximately 94.8%, 95.3%, 96.2% and 96.5%, respectively (Fig. 3). The decrease of the citric acid coating content could be observed from 5.2% to 3.5% as the post-synthesis coating temperature decreased from 90 °C to 30 °C. The formation of a citric acid coating layer on the particle surface is known to be the chemical bond formation between the carboxyl groups of citric acid on the Fe-OH sites of the iron oxide nanoparticles [28]. Since the chemical reaction rate increases with temperature, the adsorption of citric acid onto the particle surface could be enhanced by the increased coating temperature. Thus, the increased coating temperature could enhance the citric-acid coating rate, and here it was found that the sample C3-U0-90 with coating temperature of 90 °C contained the highest surface coverage of citric acid on the nanoparticles.

The average hydrodynamic sizes weighted by intensity and polydispersity values of these samples are reported in Table 2. The hydrodynamic size of C3-U0-90 (52.9 nm), C3-U0-70 (69.1 nm), C3-U0-50 (91.1 nm), and C3-U0-30 (132.9 nm) increased as the coating temperature decreased from 90 °C to 30 °C. Since the iron oxide core sizes in these samples were the same as the uncoated nanoparticles U0 (13 nm, Fig. 2d), their increased hydrodynamic size with decreased post-synthesis coating temperature could be explained by a reduction in the citric acid coating on the iron oxide cores as the temperature decreased, which was confirmed by the TGA results (Fig. 3). The nanoparticle clusters could be formed when there were not enough surfactants to keep them separated, and the clustering could increase the hydrodynamic size of nanoparticles [29]. The nanoparticles (U0) with no coating aggregated into large clusters in DI water with hydrodynamic sizes of tens of micro-meters. The size distribution of the samples is expressed in the polydispersity index (P.I.), which corresponds to the variance of the size distribution of the nanoparticles. The P.I. value of the samples with citric acid coating at different temperature, C3-U0-90, C3-U0-70, C3-U0-50, and C3-U0-30, were 0.22, 0.16, 0.25, and 0.26, respectively. However, it should be noted that the size distribution of these samples does not have a simple correlation with the citric acid surfactant coverage around nanoparticles alone. The C3-U0-90 contained the highest content of citric acid surfactant coating in these four samples as indicated by TGA result (Fig. 3) but showed less homogeneous nanoparticle size distribution (0.22) than the one of C3-U0-70 (0.16) while the C3-U0-70 displayed the smallest P.I. value among these four samples in our study. For the sample hydrodynamic size distributions, part of the dispersity was resulted from polydispersity in the single citric-acid coated iron oxide nanoparticles while some dispersity may be caused by variations in the nanocluster sizes. On one hand, the size distribution of the individual nanoparticles became narrower as the surfactant-to-water ratio decreased [24]. Thus as the content of citric acid decreased in the final products, the size distribution of the single citric acid-coated iron oxide would be

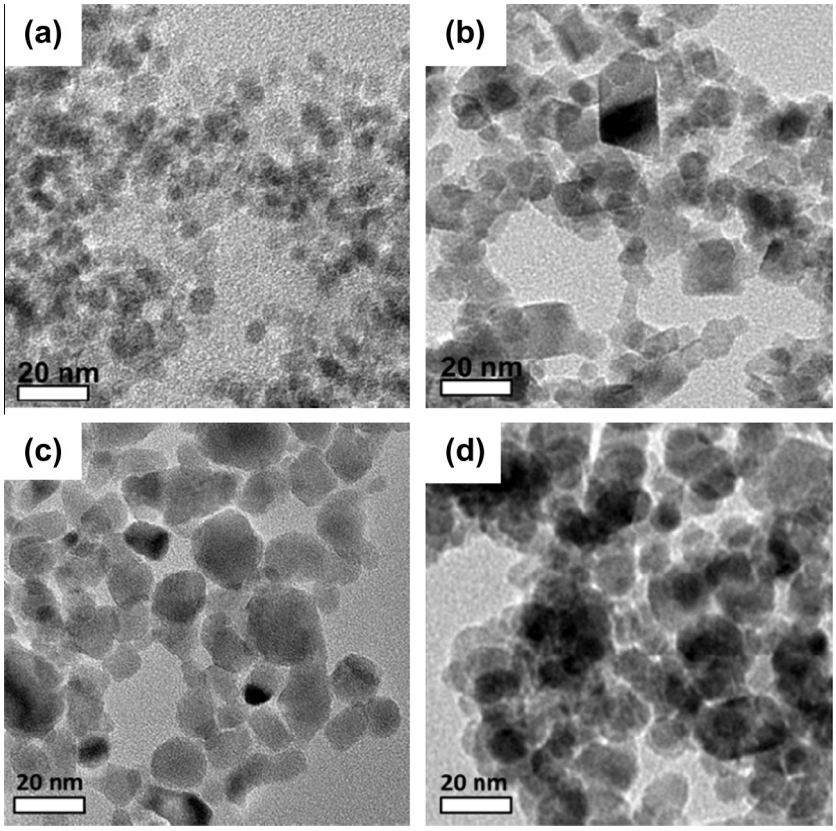

Fig. 2. TEM images of synthesized citric acid coated iron oxide nanoparticles through three methods and uncoated iron oxide nanoparticles (a) C1, (b) C2, (c) C3-U0-90, and (d) U0.

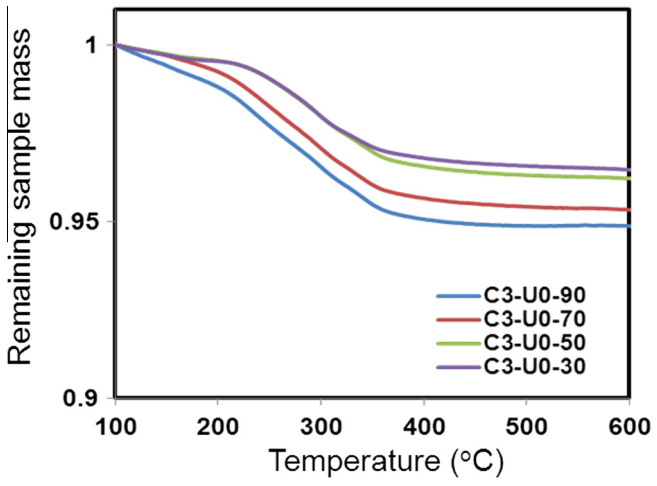

Fig. 3. TGA results of iron oxide nanoparticles coated with citric acid at different temperature in the 3rd method (C3-U0-90, C3-U0-70, C3-U0-50, and C3-U0-30).[See the electronic version of the Journal for a color version of this figure.].

narrower. On the other hand, when there were not enough surfactants to keep the nanoparticles separated, fractal aggregates could be formed with a wide size distribution [25]. As such, as the content of citric acid decreased in the final products, the size distribution of the nanoclusters would become broader. Due to these two effects, the size distribution of the final samples does not have a simple correlation with the content of citric acid surfactant coating.

Table 2
Hydrodynamic size of iron oxide nanoparticles coated with citric acid at different temperatures, in DI water.

Samples	Mean diameter[a] (nm) and polydispersity index[b]
C3-U0-90	52.9 [0.22]
C3-U0-70	69.1 [0.16]
C3-U0-50	91.1 [0.25]
C3-U0-30	132.9 [0.26]

[a] Mean particle size result from three measurements, weighted by intensity.
[b] Polydispersity index values (P.I.), given in brackets, range from 0 to 1; a higher value indicates a less homogeneous nanoparticle size distribution.

3.3. Influence of post-synthesis coating with citric acid on magnetic behavior

The influence of post-synthesis coating with citric acid at 90 °C in the 3rd method (two-step process) on the magnetic behavior of the nanoparticles was investigated on two kinds of uncoated iron oxide nanoparticles with different sizes of 9 nm (U9) and 25 nm (U25). As determined from TEM images (Fig. 4a and b), the iron oxide core sizes of the citric-acid coated samples C3-U9-90 and C3-U25-90 were still around 9 nm (mean size of sample U9) and 25 nm (mean size of sample U25), respectively. It indicates that the surfactant coating did not induce significant change of the nanoparticle core sizes. The magnetic behaviors of the samples were measured using the VSM at room temperature, as shown in Fig. 4c and d. The saturation magnetization (M_s) for the iron oxide cores of the citric acid coated samples C3-U9-90 and C3-U25-90 was determined to be 50 emu/g and 46 emu/g, almost the same as the M_s of the corresponding uncoated iron oxide nanoparticles U9 (51 emu/g) and U25 (46 emu/g), respectively. They are less than

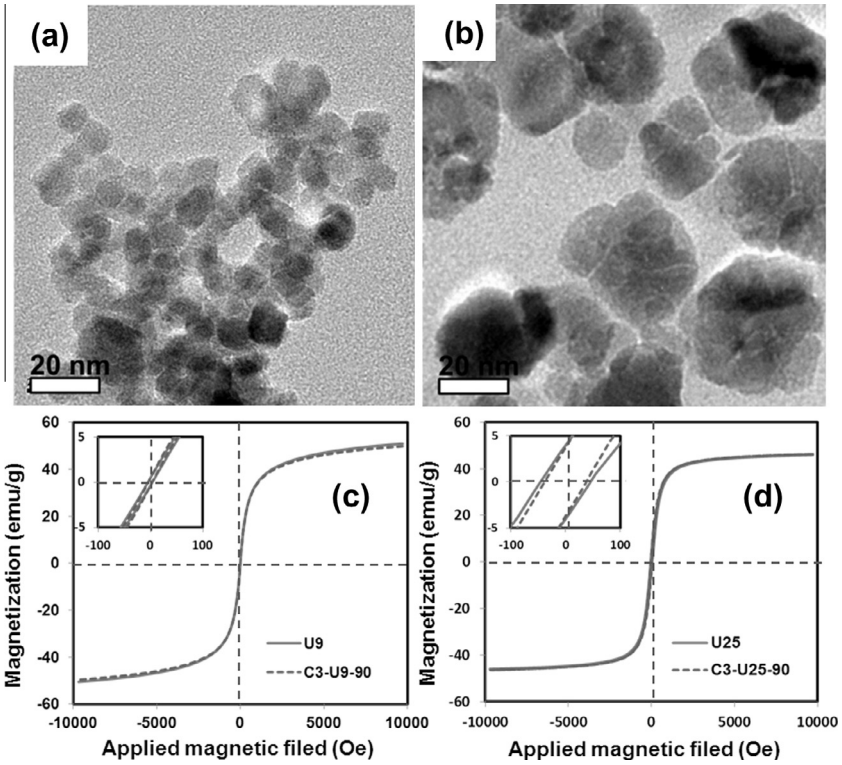

Fig. 4. TEM images and VSM results of citric acid coated iron oxide nanoparticles with core sizes of 9 nm and 25 nm in 3rd method. (a and b) TEM images of (a) C3-U9-90 and (b) C3-U25-90. (c and d) VSM results of (c) C3-U9-90 and (d) C3-U25-90. The insets in (c) and (d) are the corresponding magnified views of the M–H loops in the low magnetic field.

the M_s for bulk Fe_3O_4 (92 emu/g) and the M_s for bulk γ-Fe_2O_3 (74 emu/g) [30], but are comparable to the experimental values for M_s of magnetite nanoparticles spanned the 30–50 emu/g range [31]. The insets in Fig. 4c and d were the corresponding magnified views of the *M–H* loops in the low magnetic field. Both of the uncoated sample U9 and the citric-acid coated sample C3-U9-90 displayed a superparamagnetic behavior with negligible coercivity. The coercivity of uncoated sample U25 and citric-acid coated sample C3-U25-90 was 46 Oe and 38 Oe, respectively. The coercivity decrease of U25 after coated with citric acid could be attributed to the increased distance between the nanoparticles caused by citric-acid coating, which led to the reduction of the inter-particle dipole–dipole interaction and thus smaller coercivity [23]. For iron oxide nanoparticles with size smaller than 20 nm, the thermal energy overcomes the dipole–dipole interaction, and the thermal fluctuations can change the direction of magnetization of the entire crystal. [32] Thus, the uncoated 9-nm nanoparticles in sample U9 exhibit a superparamagnetic behavior with no coercivity at room temperature. Even though the citric-acid coating can increase the distance between the nanoparticles and reduce the inter-particle dipole–dipole interaction, the superparamagnetic nature of the 9 nm nanoparticles does not change and thus the coercivity of the citric acid coated sample C3-U9-90 stays to be zero. Therefore, the citric-acid coating did not alter the superparamagnetic behavior of the iron oxide nanoparticle with size close to 9 nm, and could reduce the coercivity of iron oxide nanoparticles with size close to 25 nm.

4. Conclusion

This study demonstrates the effect of the synthesis conditions including the addition of citric acid and the coating temperature on the properties of citric-acid coated iron oxide nanoparticles. The core sizes of the citric-acid coated nanoparticles could be adjusted from around 6 nm to 13 nm by adding the citric acid at different stage in the synthesis process: pre-addition into ferrous and ferric solution (1st method), post-addition when nanoparticles precipitated (2nd method), and post-synthesis coating after uncoated nanoparticle synthesized in a two-step process (3rd method). In the two-step process for synthesis, the decreased coating temperature resulted in increased hydrodynamic sizes of the synthesized citric-acid coated nanoparticles. Thus, the influences of the addition of citric acid and the coating temperature on the size of the final products were revealed. For the small sized (~9 nm) uncoated iron oxide nanoparticles with a superparamagnetic behavior, the citric-acid coating would not affect its superparamagnetic feature. For the larger sized (~25 nm) iron oxide nanoparticles with coercivity, the citric-acid coating would decrease their coercivity. This work indicates the synthesis conditions could be appropriately controlled to fabricate the citric-acid coated nanoparticles for a specific purpose.

Acknowledgments

This work was supported by the Seed funding Program for Basic Research from the University of Hong Kong, the RGC-GRF Grant (HKU 7049/11P), and University Grants Council of Hong Kong (contract no. AoE/P-04/08). We are thankful for the proofreading of our manuscript by Chris Roberts.

References

[1] S. Wagner, Investigative Radiology 37 (2002) 167.
[2] I. Hilger, K. Frühauf, W. Andrä, R. Hiergeist, R. Hergt, W.A. Kaiser, Academic Radiology 9 (2002) 198–202.
[3] G. Li, S. Sun, R.J. Wilson, R.L. White, N. Pourmand, S.X. Wang, Sensors and Actuators A: Physical 126 (2006) 98–106.
[4] V.K. Varadan, D.L.F. Chen, J. Xie, Wiley, 2008.

[5] A.K. Gupta, M. Gupta, Biomaterials 26 (2005) 3995–4021.
[6] J. Xie, J. Huang, X. Li, S. Sun, X. Chen, Current Medicinal Chemistry 16 (2009) 1278–1294.
[7] K. Woo, J. Hong, S. Choi, H.W. Lee, J.P. Ahn, C.S. Kim, S.W. Lee, Chemistry of Materials 16 (2004) 2814–2818.
[8] Y. Lu, Y. Yin, B.T. Mayers, Y. Xia, Nano Letters 2 (2002) 183–186.
[9] W. Wu, Q. He, C. Jiang, Nanoscale Research Letters 3 (2008) 397–415.
[10] E. Parton, R. De Palma, G. Borghs, Solid State Technology 50 (2007) 47.
[11] R. Weissleder, B.D. Ross, A. Rehemtulla, S.S. Gambhir, Molecular Imaging: Principles and Practice, People's Medical Publishing House, 2010.
[12] S. Nigam, K. Barick, D. Bahadur, Journal of Magnetism and Magnetic Materials 323 (2011) 237–243.
[13] C. Boyer, M.R. Whittaker, V. Bulmus, J. Liu, T.P. Davis, NPG Asia Materials 2 (2010) 23–30.
[14] E. Munnier, S. Cohen-Jonathan, C. Linassier, L. Douziech-Eyrolles, H. Marchais, M. Soucé, K. Hervé, P. Dubois, I. Chourpa, International Journal of Pharmaceutics 363 (2008) 170–176.
[15] K.D. Wani, R. Kitture, A. Ahmed, A.S. Choudhari, S.J. Koppikar, S.N. Kale, R. Kaul-Ghanekar, Journal of Bionanoscience 5 (2011) 59–65.
[16] M.A. Daniele, M.L. Shaughnessy, R. Roeder, A. Childress, Y.P. Bandera, S. Foulger, ACS Nano 7 (2012) 203–213.
[17] J.P. Fortin, F. Gazeau, C. Wilhelm, European Biophysics Journal 37 (2008) 223–228.
[18] L. Li, K. Mak, C. Leung, K. Chan, W. Chan, W. Zhong, P. Pong, IEEE Transactions on Magnetics 48 (2012) 3299–3302.
[19] A. Lapresta-Fernández, T. Doussineau, S. Dutz, F. Steiniger, A.J. Moro, G.J. Mohr, Nanotechnology 22 (2011) 415501.
[20] C. Liu, P. Huang, Soil Science Society of America Journal 63 (1999) 65–72.
[21] A. Bee, R. Massart, S. Neveu, Journal of Magnetism and Magnetic Materials 149 (1995) 6–9.
[22] C. Hui, C. Shen, T. Yang, L. Bao, J. Tian, H. Ding, C. Li, H.J. Gao, The Journal of Physical Chemistry C 112 (2008) 11336–11339.
[23] A. Tomitaka, T. Koshi, S. Hatsugai, T. Yamada, Y. Takemura, Journal of Magnetism and Magnetic Materials 323 (2011) 1398–1403.
[24] S. Wan, J. Huang, M. Guo, H. Zhang, Y. Cao, H. Yan, K. Liu, Journal of Biomedical Materials Research Part A 80A (2007) 946–954.
[25] R.A. Frimpong, J. Dou, M. Pechan, J.Z. Hilt, Journal of Magnetism and Magnetic Materials 322 (2010) 326–331.
[26] E. Cheraghipour, S. Javadpour, A.R. Mehdizadeh, Journal of Biomedical Science and Engineering 5 (2012) 5.
[27] C.S.S.R. Kumar, Microfluidic Devices in Nanotechnology: Applications, John Wiley & Sons, 2010.
[28] A. Hajdú, E. Tombácz, E. Illés, D. Bica, L. Vékás, Colloids for Nano- and Biotechnology (2008) 29–37.
[29] K.D. Sattler, Nanoparticles and Quantum Dots, Taylor & Francis, 2010.
[30] T. Yogo, T. Nakamura, W. Sakamoto, S. Hirano, Journal of Materials Research 15 (2000) 2114–2120.
[31] L.A. Harris, J.D. Goff, A.Y. Carmichael, J.S. Riffle, J.J. Harburn, T.G. St. Pierre, M. Saunders, Chemistry of Materials 15 (2003) 1367–1377.
[32] C.S.S.R. Kumar, Magnetic Nanomaterials, Wiley, 2009.